JOURNAL OF MATERIALS SCIENCE 20 (1985) 2828–2838

Phase transformation and impact properties of type 17-8-2 austenitic weld metals

R. A. FARRAR, C. HUELIN
Department of Mechanical Engineering, The University of Southampton, Hampshire, UK
R. G. THOMAS
Generation Development and Construction Division, CEGB, Barnwood, Gloucester, UK

The influence of stress relieving and ageing treatments in the range 600 to 900° C on the phase transformations and change in room temperature impact properties has been studied for two manual metal arc 17-8-2 weld metals. The transformation of the δ-ferrite in the range 600 to 800° C was found to conform to a classical Johnson–Mehl equation; the initial precipitates were $M_{23}C_6$ carbides followed by the intermetallic χ-phase. At higher temperatures a slower transformation rate was found suggesting a "C" curve type of behaviour and the dominant intermetallic phase changed to σ. Room temperature impact toughness values were found to change with ageing time. Below 800° C there was a consistent fall in these values which became very marked when the χ-phase developed at the γ/δ-boundaries. Above 800° C, spherodization of the carbides and intermetallic phases delayed the fall in the impact values, and led to significant increases in the early stages of ageing. Scanning electron microscopy confirmed that the change from ductile to brittle fracture mode was normally associated with the development of the σ and χ phases, but at 600° C the fall in impact properties could be atrributed to carbide development.

1. Introduction

The molybdenum containing austenitic stainless steels of the AISI 316 type have found wide applications in steam generating plants as piping and superheater tube material. In recent years they have become increasingly important in the construction of nuclear power plants. The suitability of these materials is due above all to their high resistance to creep and corrosion. In any such installations, welded joints will be areas of critical importance since their properties can differ significantly from the wrought base material.

It is now accepted practice to deposit weld metals of matching composition to the base plate, but which contain between 5 and 8% δ-ferrite in the austenitic matrix to avoid hot cracking during solidification [1].

Since stress relief heat treatments can cause the metastable δ-ferrite to transform to chromium rich $M_{23}C_6$ carbides and intermetallic phases such as σ and χ, it is essential that the kinetics of these reactions are understood and the significance they have on the tensile and impact properties as the transformation proceeds. Earlier work by Thomas and Keown [2] and Hill [3] has suggested that thermal ageing will result in reductions in impact energies. The impact energy starts lower and generally decreases at a greater rate than that of the wrought material. This has been associated with the more rapid precipitation of carbides and intermetallic phases in weld metals due to the presence of suitable nucleation sites at the δ/γ boundaries [4].

The purpose of this present paper is to describe some systematic studies of the transformation kinetics, phases developed and the changes in

0022–2461/85 $03.00 + .12

TABLE I Weld metal composition (wt %)

Weld no.	Consumable rods	Composition							Ferrite no.
		C	Cr	Ni	Mo	Mn	Si	S	
1	Metrode (RCF)	0.07	16.9	9.1	1.6	1.8	0.28	0.002	4.9
2.	ArmexGT	0.07	17.6	8.8	1.7	2.0	0.32	0.005	7.9

impact properties with ageing in the temperature range 600 to 900° C for 17-8-2 manual metal arc weld metals.

2. Experimental details

2.1. Materials

The "lean" AISI 316 type weld metals used in this study were deposited using commercial 4 mm manual metal arc rods with rutile coatings. The nominal compositions were 17% Cr, 8% Ni and 2% Mo with a controlled δ-ferrite content between 5 and 8%. The actual results obtained are given in Table I.

The welds were deposited on a mild steel base plate as a pad in the downhand position, the welding direction was always from left to right as shown in Fig. 1, to produce an aligned columnar grain structure in which the orientation of the grains with respect to the edges of the pad was constant and known.

2.2. Tensile and Charpy testing

Standard full size Charpy and tensile specimens were used to determine the mechanical properties as a function of ageing time. The Charpy specimens were machined from the weld pad so that the grains were orientated perpendicular to the long axis of the specimen, the notch was located as shown in Fig. 2 after a light electrolytic etch to reveal the exact grain orientation. The tensile specimens were extracted so that the grain orientation was along the axis of the reduced section.

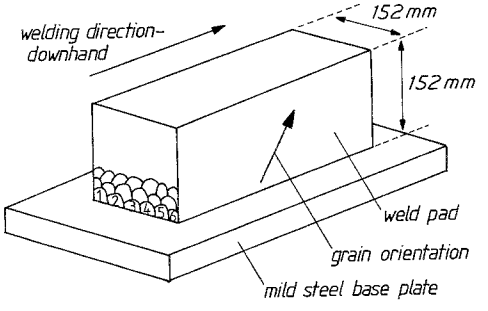

Figure 1 Standard welding pad for controlled grain orientation.

2.3. δ-ferrite transformation

Measurement of the δ-ferrite content was obtained using an Aminco-Brenner Magne Gage which had been calibrated using primary and secondary standards according to the AWS A4-2-74 calibration procedure [5]. A template of the Charpy specimens was made to ensure the specimens were located in precisely the same relative position for each determination after ageing. The values quoted are the average of 10 readings along the specimen.

2.4. Heat treatment

Specimens were aged for various times at 600 to 900° C in a horizontal tube furnace controlled to ± 2° C. After quenching the specimens in water and removing the oxide scale by light grinding on 600 grade paper, a further ten Magne Gage readings were taken for each specimen at the same locations where the initial ferrite readings were taken.

2.5. Metallographic examination

After the appropriate heat treatment, the Charpy energy or tensile properties were measured at room temperature. The broken specimens were then sectioned for metallographic examination. The fracture surfaces were mounted for examination by scanning electron microscopy, whilst part of the specimen was mounted for conventional optical microscopy following suitable polishing and etching. To supplement the optical microscopy some specimens were polished and etched for examination in the scanning electron microscope.

For a quantitative determination of all the phases present, a bulk extraction method was

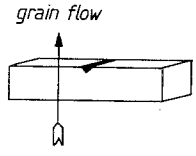

Figure 2 Location of notch with respect to grain flow.

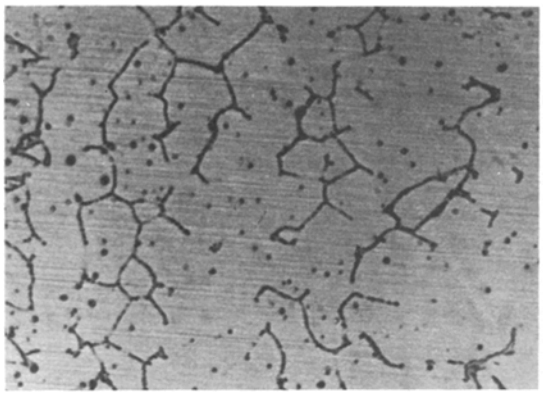

Figure 3 As-welded microstructure. Dark etching "skeletal" ferrite is located along the cores of the austenite sub grains. 10% oxalic acid etch × 650.

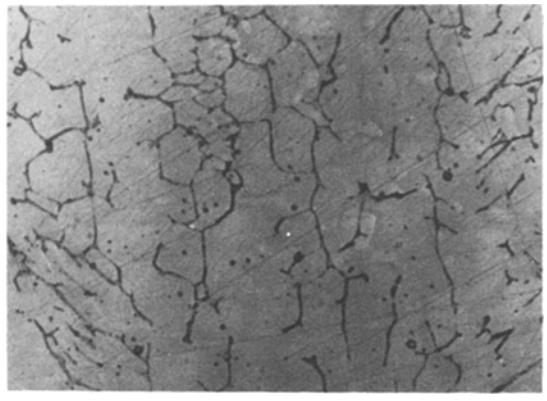

Figure 4 Change in microstructure after 0.1 h at 800° C. Some precipitation is occurring within the δ-ferrite. Modified Murakami's etch × 520.

employed using a 10% HCl-methanol electrolytic dissolution method. The non-soluble residues were washed in methanol and then centrifuged. The dried, extracted powder was then examined by the Debye–Scherrer technique using Cr$K\alpha$ radiation. Phase identification was then carried out using the ASTM powder diffraction file.

In order to determine the segregation analyses between the δ and γ phases electron microprobe analysis was performed on as-welded and certain aged samples. Owing to the very fine structure a point counting technique with a resolution of ± 2 μm was used.

3. Experimental results

3.1. Metallography

The typical as-welded microstructure is shown in Fig. 3, the ferrite occurs in a lacy, interlocked dendritic form growing perpendicular to the plane in which the freezing occurred. This type of structure is normally referred to as skeletal ferrite [6]. The dimensions and morphology of the δ/γ microstructure varied in the specimen and was found to be dependent on the weld bead shape and size and the position within the bead. Recent studies by Brooks *et al.* [7] suggest that skeletal ferrite results from a diffusion controlled reaction with partitioning of nickel to the γ and chromium to the δ, leaving a chromium-rich nickel-lean core which is then stable at room temperature. The remaining liquid then transforms to γ. This is then followed by solid state diffusion of nickel and chromium between the δ and γ phases. The final segregation profiles are thus produced by a combination of microsegregation and partitioning during the solid state reaction. A secondary feature of the as-welded microstructure was the presence of numerous deoxidation products. These tend to be oxygen-rich manganese silicates, which are known to absorb elements such as sulphur and phosphorus which contribute to hot cracking in these welds.

One of the major difficulties found in analysing the changes in the microstructure due to heat treatment was the similar etching characteristics of the different phase transformation products. The most useful etch was found to be a modified Murakami's reagent. Figs. 4 and 5 show the changes observed following ageing at 800° C. The initial stages of the phase transformation appeared to be associated with the development of carbides followed by precipitation of intermetallic χ and σ phases. At high magnifications the original

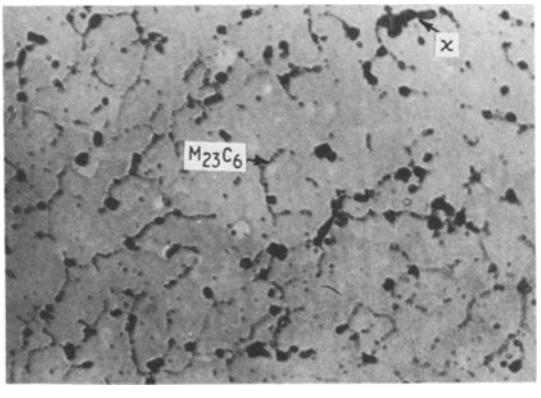

Figure 5 Change in microstructure after 960 h at 800° C. The $M_{23}C_6$ carbides (light grey) are dissolving and the χ phase (dark) is appearing. Modified Murakami's etch × 520.

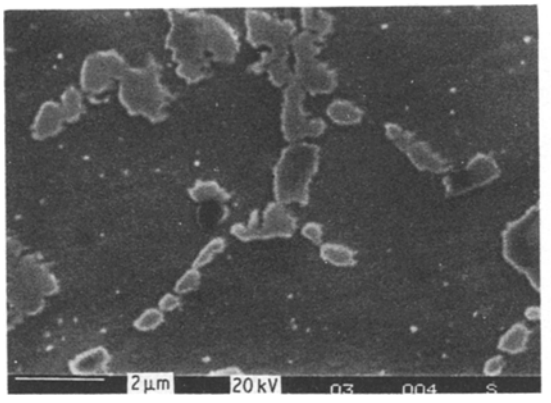

Figure 6 Scanning electron micrograph of an etched surface similar to that shown in Fig. 5, illustrating the ragged nature of the precipitate phase boundaries.

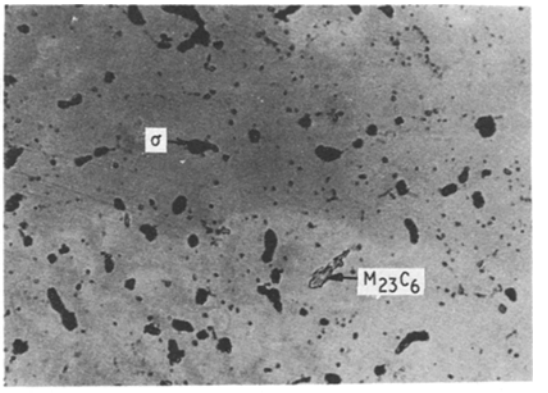

Figure 7 Change in microstructure after 66 h at 900° C. All the δ-ferrite has transformed to spherodized σ-phase plus some remaining $M_{23}C_6$ carbides. 10% oxalic etch × 325.

smooth δ/γ boundaries break down and are replaced by the ragged boundaries as illustrated in Fig. 6.

Ageing at temperatures above 800° C appeared to produce a definite spherodization in the precipitating phases. Fig. 7 illustrates this process occurring at 900° C in which it is clearly seen that the original δ-ferrite is not only transforming to a mixture of carbides and intermetallic phases, but that spherodization has also occurred.

3.2.1. Transformation kinetics 600 to 800° C

Assuming Delong's [8] conclusion that the rate of transformation of δ-ferrite is independent of the initial ferrite content, the results of the ageing experiments at 600 to 700 and 800° C are shown in Fig. 8. The transformation curves are clearly sigmoidal in shape and can be fitted to a standard Johnson–Mehl equation of the form:

$$x = 1 - \exp(-bt^n)$$

where x is the fraction of δ-ferrite transformed and b and n are constants.

Using simple linear regression analysis, the value of n for this current data was found to be 0.337. The temperature dependence of the transformation process was investigated by determining if the results were compatible with an Arrhenius equation. This was found to be true for the 600 to 800° C temperature range and gave a value for the activation energy of 399 kJ kg^{-1} mol^{-1}.

The fitting of this equation to the results obtained at 800° C is shown in Fig. 9, which indicates an excellent correlation between the theoretical and experimental data.

3.2.2. Transformation kinetics 850 to 900° C

Although the transformation behaviour was similar to the 600 to 800° C regime and displayed a sigmoidal shape, Fig. 10, the kinetics

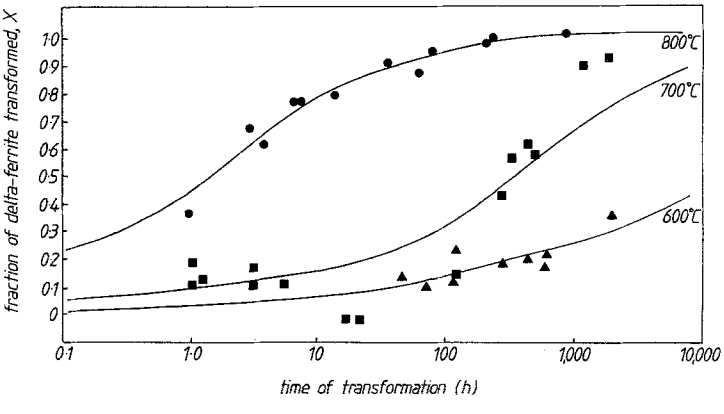

Figure 8 δ-ferrite transformation curves at 600, 700 and 800° C.

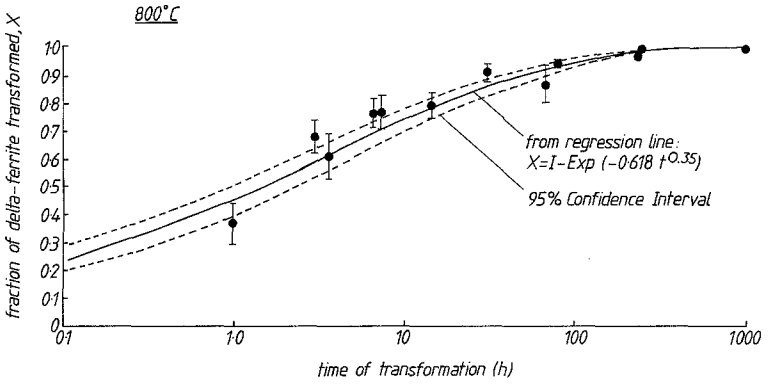

Figure 9 δ-ferrite transformation curve at 800° C. The curve has been fitted by least squares to Johnson–Mehl equation $x = 1 - \exp(-bt^n)$.

had changed and the reactions had slowed up compared with those measured at 800° C. This suggests that either a new precipitation reaction was occurring or the transformation follows a "C" curve behaviour [9].

3.3. Tensile and hardness results

The tensile tests carried out gave results which compared well with previous work. These together with the hardness results are shown in Table II. In the lower temperature regime there appears to be a slight increase in the hardness values with ageing time consistent with a progressive precipitation reaction, but at temperatures above 800° C any precipitation reaction is offset by a softening reaction which leads on balance to a reduction in strength and hardness.

3.4. Impact testing

The results of full size Charpy testing are given in Table III. Fig. 11 illustrates the changes that have occurred with ageing by plotting the impact results as a percentage change from the as-welded value of 90 J. At temperatures above 800° C a reversal in the trend was seen and a definite increase in the impact energy was observed in the early stages of ageing. Eventually the impact properties began to decrease to the as-welded value, but at 900° C this had not occurred after 120 h ageing. Although two slightly different weld metals were used in this investigation it can be seen from Fig. 11 that the two sets of results at 800° C are consistent with each other.

3.5. Fractography

The variations in the fracture modes were observed using the scanning electron microscope, this displayed a change from fully ductile to fully brittle as the transformation proceeded in the lower temperature regime. The as-welded material, Fig. 12, displayed a typical ductile dimple surface with microvoid coalescence occurring around the deoxidation inclusions, a similar ductile fracture was observed after 0.1 h ageing at 800° C. After 14 h, however, in which the precipitation of $M_{23}C_6$ carbides had begun to occur the fracture surface began to change and show signs of small cleavage areas as illustrated in Fig. 13.

As the ageing times at 800° C were increased, the fracture surface increasingly became more

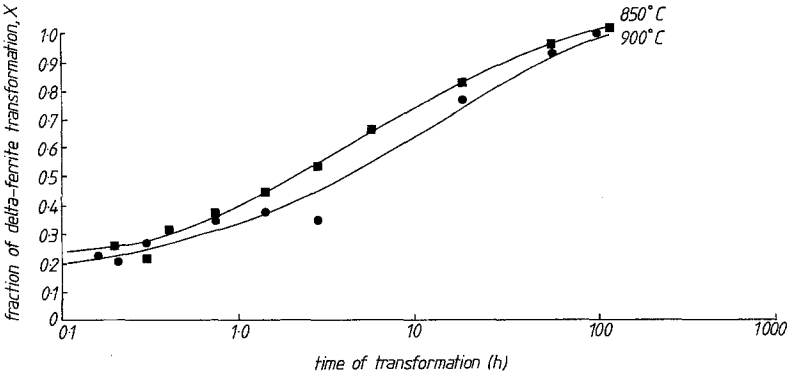

Figure 10 δ-ferrite transformation curves at 850 and 900° C.

TABLE II Ultimate tensile strength, UTS, in MN m^{-2}, and hardness, VPN, at 10 kg. VPN values given in parenthesis

As-welded ⟶	610 (230)			
	Time (h)			
Temperature (° C)	10	72	120	1000
600	– (230)	–	– (230)	– (250)
700	– (230)	–	– (240)	– (245)
800	– (220)	–	– (240)	– (245)
850	– (230)	600 (250)	–	–
900	–	565 (220)	577 (220)	–

– not determined

brittle with definite cleavage and microcracks being observed, Fig. 14. As the amount of the intermetallic phases increased still further, the fracture surface became totally brittle with only very small areas of ductile tearing occurring between the cleavage facets, Fig. 15.

Ageing at temperatures above 800° C produced similar changes in the fracture behaviour but within differing time scales, at 850° C a fully brittle fracture behaviour was observed after only 66 h ageing, Fig. 16. By contrast welds which were aged at 900° C, and had displayed an initial increase in impact energy were found to be highly ductile after 66 h ageing. This appears to be consistent with the changes in impact behaviour shown in Fig. 11.

3.6. Phase indentification

The results obtained from the diffraction patterns were compared with the values given in the ASTM data file using a simple visual calibration film to assess the relative intensities of the diffraction lines. The variation in the phases identified and their relative quantities are shown in Table IV. It is interesting to notice the presence of $M_{23}C_6$ carbides in the as-welded material, presumably due to reheating by successive beads in a multi-pass weld metal.

3.7. Electron microprobe analysis

The variations in the chromium and nickel contents across the austenite δ sub-boundaries in the as-welded and aged samples are shown in Fig. 17a and b. The electron microprobe resolution is limited by beam spreading to the order of 2 to 3 μm, nevertheless the results show the definite enhancement of the chromium level in the δ-ferrite which increases on ageing for long times at 800° C. This is consistent with the recent work of Farrar and Thomas [10] on similar types of weld metals.

4. Discussion

4.1. Phase transformation of δ-ferrite

Considering the rate of transformation for a 50% transformation of the δ phase, which implicitly assumes that the number of nuclei formed is independent of temperature and that only the growth mechanism is being considered, it is possible to derive an equation to describe the transformation results in the temperature range. This is as follows:

$$\ln[-\ln(1-x)] = 14.461 - \frac{16141}{T} + 0.337 \ln t$$

This equation is similar in form to that reported by Thomas and Keown [2], with the change in the numerical values resulting from the different curve fitting used in the two investigations. At

TABLE III Impact properties (J)

As-welded ⟶	90						
	Time (h)						
Temperature (°C)	0.1	1.0	5	10	120	500	1000
600	90	85	83	78	75	75	68
700	90	85	83	78	75	60	50
800	85(88)	83(83)	80(77)	75(69)	48(43)	35(25)	27(–)
850	(117)	(103)	(88)	(80)	(60)	–	–
900	(101)	(113)	(124)	(128)	(117)	–	–

( ) Results from Alloy 2.

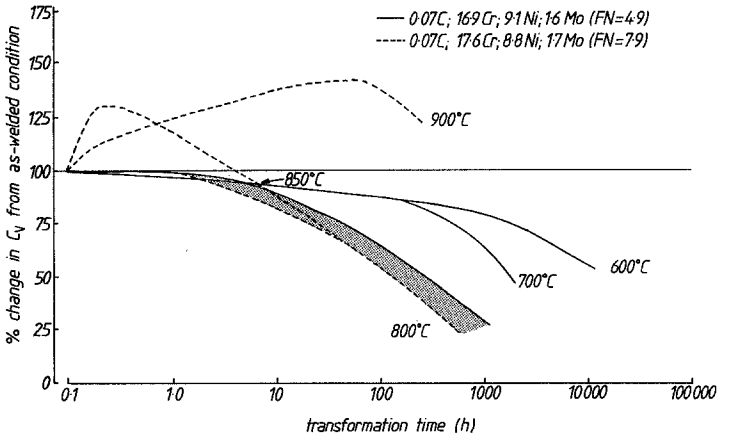

Figure 11 % change in room temperature impact properties after heat treatment at 600, 700, 800, 850 and 900° C.

temperatures above 800° C, the present work indicated a distinctive change in the transformation kinetics. The "C" curve type of behaviour has been observed in many systems and has been reported for 316L wrought materials by Weiss and Stickler [9].

These authors argued that the increased stability of the material against intermetallic phase formation at the higher temperatures resulted from the stabilization effect of the greater solubility of carbon in the austenite matrix. The results of the present study are shown in the form of a T–T–P diagram, Fig. 18, together with suggested phase boundaries for the σ and χ phases. This figure is similar to that presented by Weiss and Stickler for 316L wrought materials, but it is interesting to notice the shorter times required for precipitation due to the increased number of suitable nucleation sites. Unlike Weiss and Stickler there was no evidence for η phase formation in these present studies.

TABLE IV δ-ferrite phase transformation products

Condition	Phases detected		
	$M_{23}C_6$	χ	σ
As-welded ⟶	xx	–	–
Aged			
600° C for 2000 h	xxx	–	–
20 000 h	xxxx	–	–
700° C for 300 h	xxx	–	–
2 000 h	xx	xx	–
800° C for 0.1 h	xxx	–	–
14 h	xxx	–	–
90 h	xx	xx	–
960 h	xx	xx	x
850° C for 0.2 h	xx	–	–
1.5 h	xx	–	x
3 h	xx	x	x
6 h	xx	x	xx
66 h	x	xx	xx
900° C for 0.1 h	xx	–	–
0.8 h	xx	–	–
1.5 h	xxx	–	–
3 h	xxx	–	x
20 h	xx	–	xx
66 h	x	–	xx
120 h	x	–	xxx

x → xxxx Increased frequency.
– Below detection limit.

Thomas and Keown have studied a very similar 17-8-2 weld metal [11] and they reported that the σ/carbide boundary existed as some 50 to 75° C below that shown in Figure 18. This difference may be due to their use of electron diffraction to identify the phase changes and slightly different δ-ferrite segregation compositions.

The present results together with those of Thomas and Keown [11] indicate that the transformation of the δ-ferrite is controlled by the diffusion of both the carbon in the austenite matrix and the substitutional elements such as chromium and nickel within the δ-ferrite.

The electron microprobe evidence for the changes in the chromium and nickel concentrations is consistent with the recent work of Farrar and Thomas [10] on a series of 19-12-3 weld materials. These authors observed very clear changes in the composition of the δ-ferrite as a function of ageing time.

4.2. Room temperature impact and tensile properties.

Most published work has linked the marked reduction in room temperature impact energy after long ageing times to the formation of the σ-phase.

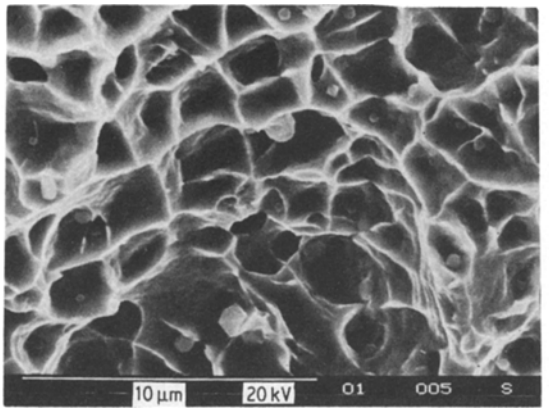

Figure 12 Ductile fracture surface of the as-welded material showing microvoid initiation at weld metal inclusions.

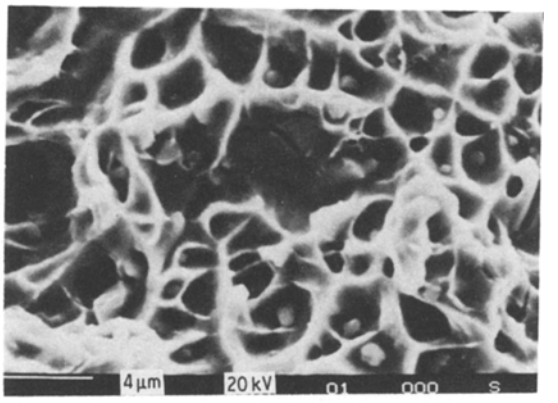

Figure 14 Fracture surface after 960 h at 900° C. Increased brittle fracture facets associated with the development of the χ-phase.

Fig. 11 shows that the 17-8-2 weld metal studied in this work does not suffer a significant reduction in room temperature impact energy after heat treatment at 600° C for times up to 5000 h. The 25% drop in impact energy observed was found to be associated with the increased precipitation of $M_{23}C_6$ carbides. After 300 h at 700° C, during which some 55% of the δ-ferrite had transformed, the impact energy had fallen slowly to 75 J. Again phase analysis confirmed that the only precipitated phase was $M_{23}C_6$. Further ageing at this temperature resulted in a sharp drop in the impact energy to 44 J due to the rapid precipitation of the intermetallic χ-phase.

A similar reduction in impact energy was observed in the samples aged at 800° C but only after 14 h of heat treatment. Again the initial precipitation of $M_{23}C_6$ carbides did not greatly reduce the impact energy, but the rapid precipitation of χ-phase caused a reduction to 27 J after 100 h ageing. Thomas and Keown [2] had concluded that the reduction in impact properties at 800° C was due to the precipitation of the σ-phase. In both cases, however, the rapid reduction in impact energy may be ascribed to the precipitation of intermetallic phases.

At temperatures above 800° C there was a rapid rise in the impact energy during the early stages of ageing. The present results suggest that although there is a rapid precipitation of carbides from the δ-ferrite which would produce a reduction in the impact properties, the process of spherodization of the precipitate phases occurs which restricts the possibility for crack propagation, and on balance leads to a rise in the impact energy.

After this early stage, the precipitation of σ dominates the fracture process and the Charpy energy falls very rapidly, so that after 20 h the

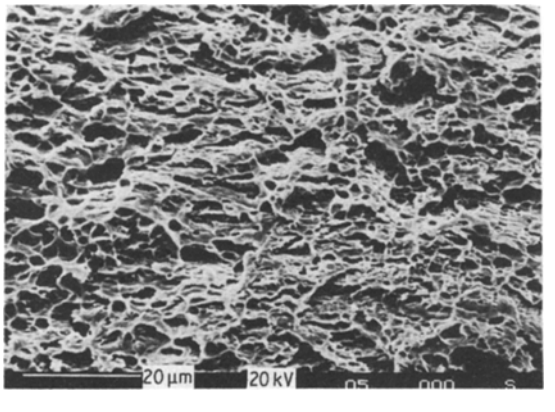

Figure 13 Fracture surface after 14 h at 800° C. The precipitation of carbides has led to some reduction in ductility.

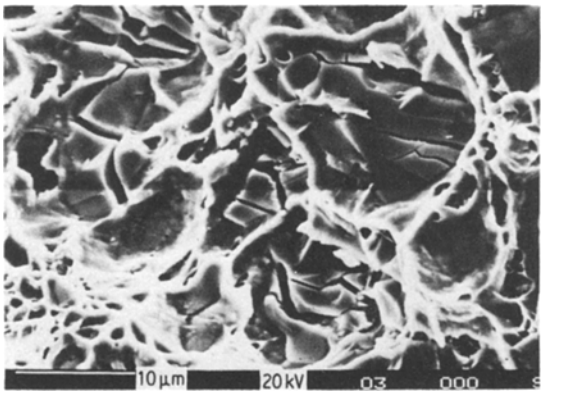

Figure 15 Fracture surface after 960 h at 800° C. Virtually all brittle fracture associated with the χ-phase.

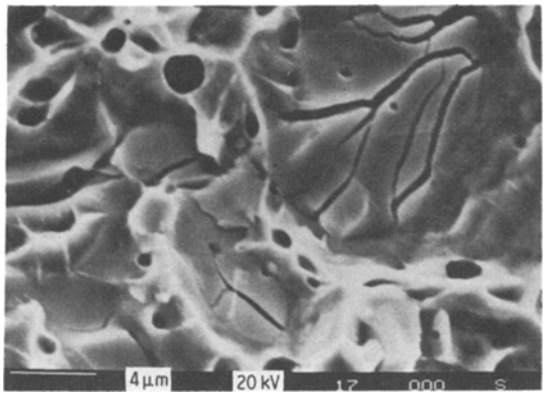

Figure 16 Fracture surface after 66 h at 850° C. Severe microcracking associated with the presence of σ and χ-phases has led to a drastic fall in ductility.

weld has the same impact energy as the material aged at 800° C. This is clearly seen in Fig. 16 which shows a totally brittle fracture surface after 66 h ageing at 850° C due to presence of both χ and σ phases.

At 900° C the initial rise in the impact energy persisted over a much longer time period. Only after ageing for 120 h was there any indication of a reduction in the impact properties.

Optical examination revealed that both the carbide and the intermetallic σ phases were highly spherodized. No χ phase was detected at this temperature. It is suggested that the process of spherodization dominates the microstructural changes at these temperatures and compensates for the production of the brittle σ intermetallic phase. Certainly the fracture surface after 66 h at 900° C is completely different to that observed after the lower temperature ageing. Fig. 19 reveals a completely ductile surface similar to that observed with the as-welded material.

TABLE V Combination heat treatments

Temperature and time	Phases observed			Impact energy, % change
	$M_{23}C_6$	χ	σ	
900° C (72 h) + 850° C (72 h)	xxx	x	xx	+ 23
850° C (72 h) + 900° C (72 h)	xx	x	xx	+ 56
1050° C (1.5 h)	–	–	–	+ 86

4.3. Combined heat treatments

In order to explore further the effect that spherodization was having on the room temperature impact properties, two combined heat treatments were performed. The results in Table V reveal significant differences between the single and double ageings. In the case of the weld aged initially at 850° C, the single ageing produced a 30% drop in impact resistance, but the double heat treatment reversed this effect and produced a 56% increase. Clearly at 900° C the spherodization of the initial carbides and intermetallics is dominant and has produced a ductile mode of fracture. In the case of the weld aged at 900° C, the single ageing produced a 35% rise in impact energy, whereas the double ageing only produced a slight modification with 23% increase on the as welded values. This is not surprising as the degree of spherodization would be less at the lower temperature.

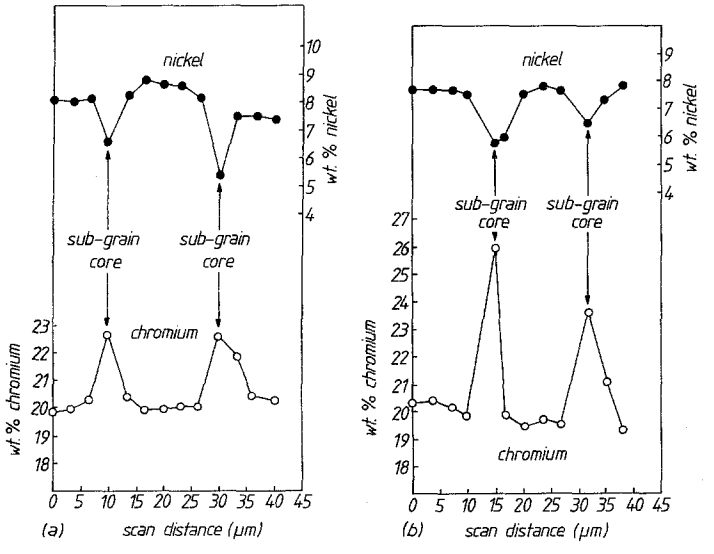

Figure 17 Electron microprobe analysis trace across ferrite/austenite boundaries in the as-welded condition. (b) Similar trace across original ferrite/austenite boundaries after 960 h at 800° C. Notice the increased chromium content associated with the χ-phase precipitation.

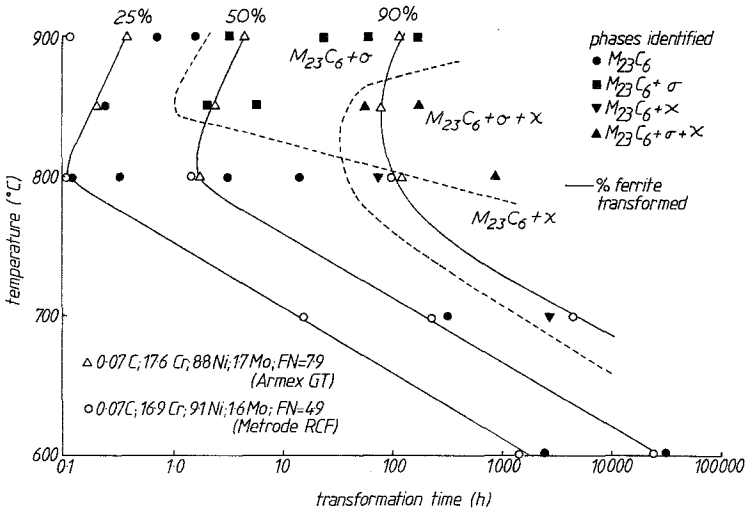

Figure 18 Time–temperature–precipitation diagram for 17-8-2 manual metal arc weld metals.

Finally it is interesting to observe that when the weld material is solution treated to dissolve all the carbides and intermetallics, there is an 86% increase in impact energy.

4.4. Embrittlement mechanisms

Farrar and Thomas [1] have shown that there is a very rapid diffusion of carbon in the γ matrix to the carbides nucleating at the δ/γ boundaries. If we assume that all the chromium for the $M_{23}C_6$ carbides comes from the δ it is obvious that the concentration profiles will change very little during the initial carbide precipitation. The transformation must now be controlled by the diffusivity of chromium away from the lath into the advancing interface bowing out from the carbides. Biss and Cryderman [12] have explained the precipitation of carbides in the C–Mn steels, they suggest that as the weld solidifies the carbon diffuses away from the ferrite to the austenite owing to the greater solubility in the f c c matrix, and it is this carbon concentration that is available on stress relieving or reheating. The grain-boundary carbide films formed are normally considered to offer easy crack propagation paths. The results of this work have shown, however, that carbide precipitation is responsible for only a small drop in impact strength. It is suggested that carbide formation is only detrimental when the films reach a certain size and thickness, below this size they can bend and deflect. As they grow and thicken, deflection can no longer occur and easy crack propagation results [13]. This is probably the case with the material aged at 600° C for 3000 h.

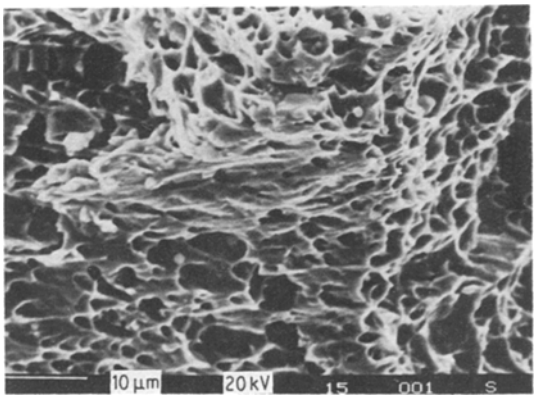

Figure 19 Fracture surface after 66 h at 900° C. Spherodization of the carbides and intermetallics has produced increased ductile fracture compared with the as-welded state.

Previous work has shown that the development of the intermetallic phases such as σ and χ depend upon the exact concentrations of chromium and molybdenum remaining in the δ-ferrite once the carbides have been formed [10]. Once these intermetallic phases develop they will provide easy crack paths in the structure and the impact properties will deteriorate as is observed in the material aged at 800 and 850° C. If, however, a spherodization of these phases occurs as is the case with the material aged at 900° C then the easy crack paths are removed and only a small drop in impact properties will be observed.

5. Conclusions

1. 17-8-2 stainless steel weld metal solidifies as primary skeletal ferrite. The δ-ferrite is enriched

in chromium and molybdenum and depleted in nickel.

2. The rate of transformation in the temperature range 600 to 800° C may be described by a Johnson–Mehl equation of the form:

$$\ln[-\ln(1-x)] = 14.461 \frac{16141}{T} + 0.337 \ln t$$

3. The transformation conforms to an Arrhenius type reaction with an activation energy of 399 kJ kg^{-1} mol^{-1}.

4. X-ray analysis revealed that the as-welded samples contained significant amounts of $M_{23}C_6$ carbides. These were probably produced by the reheating of a particular bead by successive runs in a multipass weld.

5. At 600° C, only carbides were found as the precipitated phases after 20 000 h of ageing. At 700° C, ageing for 2000 h produced carbides and χ phases in equal proportions. At 800° C, ageing for 100 h produced both carbides and the χ-phase, after 1000 h some evidence for the σ-phase was obtained. At 850° C, ageing for only 1.5 h produced some σ-phase and after 60 h there were equal proportions of σ and χ phases. At 900° C σ was the only intermetallic phase formed after 3 h ageing.

6. The precipitation reactions may be described by a "C" curve.

7. At 600° C the fall in the impact energy values after 1000 h may be ascribed to the development of thick carbides at the δ–γ boundaries.

8. At temperatures of 700° C and above, the marked reduction in the impact energy may be attributed to the precipitation of the intermetallic χ and σ phases.

9. At 850 and 900° C a spherodization reaction was found to occur which produced initial increases in the impact energy. At longer ageing times this reaction was found to limit the eventual reduction in the impact energy due to intermetallic formation.

Acknowledgements

The authors are grateful for the data provided by R. Bankart and to the Laboratory Manager Marchwood Engineering Laboratories CEGB for the provision of some laboratory facilities.

References

1. F. C. HULL, *Weld. J. Res. Suppl.* **46** (1967) 339.
2. R. G. THOMAS and S. R. KEOWN, "Mechanical Behaviour and Nuclear Applications of Stainless Steel at Elevated Temperatures", Varese Conference, May 1981 (Metals Society, London, 1982) Book 280, p. 30.
3. F. C. HULL, *Weld. J. Res. Suppl.* **52** (1973) 1045.
4. C. A. P. HORTON, P. MARSHALL and R. G. THOMAS, "Mechanical Behaviour and Nuclear Applications of Stainless Steel at Elevated Temperatures", Varese Conference, May 1981 (Metals Society, London, 1982) Book 280, p. 66.
5. W. T. DELONG, *Weld. J. Res. Suppl.* **52** (1973) 69.
6. H. FREDERIKSSON, *Met. Trans.* **3** (1972) 2989.
7. J. A. BROOKS, J. C. WILLIAMS and A. W. THOMPSON *ibid. A* **14A** (1983) 1271.
8. W. T. DELONG, *Weld. J. Res. Suppl.* **53** (1974) 286.
9. B. WEISS and R. STICKLER, *Met. Trans.* **3** (1972) 851.
10. R. A. FARRAR and R. G. THOMAS, *J. Mater. Sci.* **18** (1983) 3461.
11. R. G. THOMAS and S. R. KEOWN, CEGB Report RD/M/R312 (1981).
12. V. BISS and R. L. CRYDERMAN, *Met. Trans.* **2** (1971) 226.
13. R. C. COCHRANE, Proceedings of Conference, "The effect of Second Phase on the Mechanical Properties of Steel", Scarborough, March 1971 (Iron and Steel Institute, London, 1971) p. 101.

Received 21 August
and accepted 13 September 1984